Desirable arrangement of thermoelectric modules for radiant cooling panel

Conference Paper · July 2018

CITATIONS
0

READS
1,029

2 authors:

Hansol Lim
University of Nottingham
44 PUBLICATIONS **132** CITATIONS
SEE PROFILE

Jae-Weon Jeong
Hanyang University
146 PUBLICATIONS **1,955** CITATIONS
SEE PROFILE

Desirable arrangement of thermoelectric modules for radiant cooling panel

Hansol LIM and Jae-Weon JEONG*

Hanyang University, Department of Architectural Engineering, Seoul, Republic of Korea
jjwarc@hanyang.ac.kr

* Corresponding Author

ABSTRACT

The thermoelectric module-based radiant cooling panel (TEM-RCP) has attracted attention as an alternative for conventional hydraulic radiant cooling panels because of its advantages of no refrigerant, no chemical reactions, and no moving parts. In addition, it has merits of easy control and fast response through direct heat absorption from TEM without water. However, there are few guidelines for designing the TEM-RCP and no study has yet suggested how to arrange the thermoelectric modules (TEMs) for the radiant cooling panel. Therefore, this study proposes a desirable arrangement of thermoelectric modules for the radiant cooling panel by developing the design methods for the TEM-RCP based on the semi-black box model of TEM and the two-dimensional finite difference method. A mock-up model of the TEM-RCP was constructed to validate the proposed model and results. The constructed TEM-RCP was composed of seven TEMs, an aluminum plate, a heat sink attached to the TEMs, duct, and fan. The panel temperature at the aluminum radiant panel was maintained at 16 °C. The rejected heat from the hot side of TEM was removed by outdoor air. The design point we focused on herein was the panel temperature distribution according to the American Society of Heating, Refrigerating and Air-Conditioning Engineers Handbook. Therefore, the optimal array and the distance between the TEMs must not exceed the maximum temperature difference of 3°C across a given grid. As a result, the triangular grid was found as the best grid for an even temperature distribution of the TEM-RCP. The optimal distance between the TEMs was 0.2 m to 0.3 m according to the room condition and operation characteristics of the TEM. The optimized results were verified using the mock-up model of the TEM-RCP in the experiments.

1. INTRODUCTION

The decoupled system concept of ventilation and parallel sensible cooling has attracted much attention because of its benefits, including energy conservation and indoor air quality (Jeong et al., 2003). Among the parallel sensible cooling units, the ceiling radiant cooling panel (CRCP) is popular because it is a comfortable, efficient, and quiet cooling system. A conventional CRCP uses water chilled by a vapor compression system, which uses refrigerants. This system shows good energy efficiency; however, present refrigerants have a global warming potential (GWP) and an ozone depletion potential (Kim et al., 2016).

As an alternative solution, the thermoelectric module (TEM) is studied as a non-vapor compression technique without a refrigerant. The air-cooled-type TEM radiant cooling panel (TEM-RCP) with a solar panel was developed, and its performance when used with the displacement ventilation system was estimated (Liu et al., 2014). An in situ air-cooled-type TEM-RCP was constructed. This TEM-RCP can be operated under a COP of 0.9 for cooling and 1.9 for heating. However, the practical design of the TEM-RCP has not yet been described. Lim et al. (2017) proposed a dedicated outdoor air system (DOAS) with a water-cooled-type TEM-RCP. Based on the detailed energy simulation, the water-cooled TEM-RCP with DOAS can save approximately 44.5% of energy compared with the conventional variable air volume system. By considering the water-cooled-type TEM-RCP, the previous studies revealed the feasibility of using TEM-RCP in both air- and water-cooled types. However, the practical design for TEM-RCP still has limitations.

Luo et al. (2016) recently developed a dynamic two-dimensional (2D) analytical model for TEM-RCP using a virtual image method and artificial neural networks to predict the thermal resistances. The results proposed the optimal thickness of panel and insulations with an optimal distance between TEMs. The developed model showed good agreement, but was limited because the proposed optimal values for design were only for their TEM-RCP. In addition, the simulation model included the training data; therefore, it was difficult to use. Shen et al. (2017) tried to overcome

these limitations by clarifying the design procedure of TEM-RCP. The one-dimensional (1D) analytical model was constructed, and the optimized thickness of the radiant panel and the number of TEMs in a square meter were proposed. The design procedure was well developed for practical use; however, the model only considered the 1D temperature distribution of the panel. Therefore, the design of optimal arrangements for TEMs on the radiant panels is lacking. This study developed 2D simulation models for air-cooled-type TEM-RCP based on the theoretical heat transfer model for conduction and convection using the finite difference method (FDM). The developed simulation models were designed as a graphical user interface (GUI) design to provide a reliable and easy-to-use simulation tool for TEM-RCP research and development. We constructed a mock-up model of the air-cooled-type TEM-RCP to validate the simulation model and estimated the effects of TEM arrangements.

2. THERMOELECTRIC MODULE RADIANT COOLING PANEL

The TEM-RCP was used to handle the sensible cooling load in the zone. As shown in Figure 1, the TEM consists of n- and p-type semiconductors as the thermocouple and operated based on the Peltier effect. Heat was transferred from the cold side to the hot side using electrical power (Lee, 2016). The radiant cooling panel installed at the ceiling of the zone can be cooled based on the Peltier effect (Figure 2). The TEM was a solid-type heat pump; therefore, heat rejection occurred at the hot side of the TEM. The rejected heat can be removed using outdoor air to maintain the TEM performance.

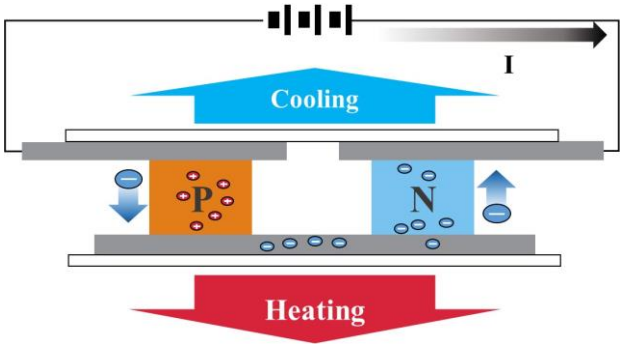

Figure 1: Principle of the Peltier effect in the thermoelectric module

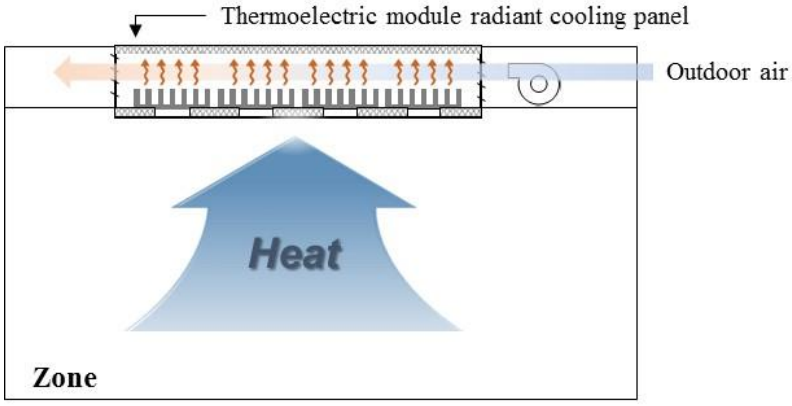

Figure 2: Schematic of the thermoelectric module radiant cooling panel in the zone

Figure 3 shows the section diagram of the TEM-RCP composed of an aluminum panel, a copper panel, insulations, TEMs, and heat sink consisting of heat pipes and fins. The cold side of the TEMs was attached to the copper panel. An aluminum panel was bonded on the copper panel. The bonding was conducted using bolts and nuts based on the compressive force; therefore, the copper panel was necessary to reduce the mechanical stress on the TEM when the volume of the aluminum panel was changed according to the temperature variations. The copper panel contributed to the uniform temperature distribution of the external panel (i.e., aluminum panel) for radiant cooling. At the hot side of the TEMs, the heat sink was installed for heat rejection to the outdoor air. The air side of the TEM-RCP must also be insulated to reduce the undesirable heat transfer to the air.

The main heat transfer in the TEM-RCP, which was related to the aluminum panel in the vertical direction, occurred based on the heat conductance between the cold side of the TEM and the bottom surface of the aluminum panel at point 1 of Figure 2. Heat conductance was observed between the top surface and the bottom surface of the aluminum panel at point 2 of Figure 2. In the vertical direction heat transfer, heat convection was observed between the surface of the aluminum panel and the room air. We assumed that no circulation fan was present in the room; therefore, natural convection occurred at the panel surface. The thermal grease between the TEM, the copper panel, and the aluminum panel was used to minimize the contact thermal resistance. We investigated the 2D temperature responses of the panel, including heat conductance between the surface temperature points of the aluminum panel in the horizontal direction.

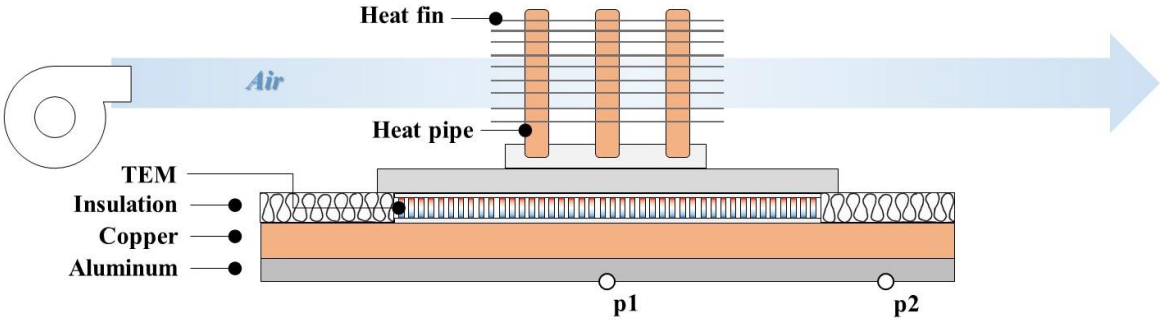

Figure 3: Section diagram of the thermoelectric module radiant cooling panel

3. SIMULATION MODEL

3.1 Thermoelectric module model

The TEM was simulated using a previously developed semi-black box model (Chen and Snyder, 2013). The thermophysical characteristics of the n- and p-type semi-conductors, including Seebeck coefficient (α), electrical resistivity (ρ), and thermal conductivity (κ), were derived using Eqs. (1) to (3), respectively. The n- and p-type thermoelements were assumed to have the same properties. The TEM properties were calculated based on the thermoelement characteristics using Eqs. (4) to (6). These equations required the technical specifications of the TEM (Table 1). The TEM used had a fraction of the total TEM area covered by a thermoelement (f_p) of 0.5 when the 127 thermocouples (N) in a TEM. We designed the mock-up model of the TEM-RCP with seven TEMs; however, the TEM in the simulation was assumed to be three to reduce the processing time.

$$\alpha = \frac{Q_{max}(T_h - \Delta T_{max})}{NT_h^2 I_{max}} \tag{1}$$

$$\rho = \frac{A_{TEM} f_p (T_h - \Delta T_{max})^2}{2T_h^2 l} \frac{Q_{max}}{N^2 I_{max}^2} \tag{2}$$

$$\kappa = \frac{l(T_h - \Delta T_{max})^2}{A_{TEM} f_p T_h^2} \frac{Q_{max}}{\Delta T_{max}} \tag{3}$$

$$S = 2N\alpha \tag{4}$$

$$R = \frac{4N^2 l}{A_{TEM} f_p \rho} \tag{5}$$

$$K = \kappa \frac{A_{TEM} f_p}{l} \tag{6}$$

Table 1: Technical specifications of the TEM used in this study

Description	Value
Dimension	40 mm × 40 mm × 3 mm
I_{max}	11.3 A
V_{max}	27.3 V
Q_{max}	188.7 W
ΔT_{max}	78°C

In the simulation, the hot-side temperature of TEM (T_h) was assumed to be 6°C higher than the air temperature for heat rejection. This assumption affected the energy consumptions of the TEM and the fan. Therefore, it can be adjusted according to the outdoor air condition and the sensible cooling load in the zone. The cold-side temperature of the TEM (T_c) was determined based on the target surface temperature of the TEM-RCP (T_{surf}), the required cooling capacity of the TEM-RCP (Q_c), and the overall heat transfer coefficient of the panel ($U_{panel-TEM}$). The surface temperature of the TEM-RCP was set as 16°C, which was lower than the annual dew point temperature of the zone, to prevent the condensation problem. We also considered the overall heat transfer coefficient consisting of the aluminum panel and the copper panel, as shown in Eq. (7). The contact thermal resistance was assumed to be negligible. Consequently, the cold-side temperature of the TEM can be derived using Eq. (8).

$$U_{panel-TEM} = \left(\frac{th_{Al}}{\kappa_{Al}} + \frac{th_{Cu}}{\kappa_{Cu}}\right)^{-1} \tag{7}$$

$$T_c = T_{surf} - \frac{Q_c}{U_{panel-TEM} A_{TEM}} \tag{8}$$

3.2 Finite difference model

The 2D finite difference model separated the component into many control volumes and solved the differential conservation and heat transfer equations within each control volume. The governing equation for the surface, which was directly faced with the TEM (point 1, Figure 2), is presented in Eq. (9). According to the TEM-RCP composition, the material properties can be adjusted in the GUI; however, the equation was described based on the TEM-RCP constructed herein. The heat convection coefficient between the panel surface and the room air ($h_{panel-room}$) was derived using Eqs. (10) to (13) (Cengel, 2007; Ostrach, 1952; Fuji et al., 1972). The heat convection at the aluminum panel was natural convection; therefore, the Grashof number (Eq. (10)) should be considered in calculating the Rayleigh number (Eq. (11)) and the Nusselt number (Eq. (12)). The characteristic length (L_c) was calculated with regard to the area of the aluminum panel.

$$\rho_{Al} C_{p,Al} \frac{\partial T}{\partial t} = \kappa_{Al} \left(\frac{\partial^2 T}{\partial x^2} + \frac{\partial^2 T}{\partial y^2}\right) + \frac{h_{panel-room}}{th_{Al}} (T_{room} - T_{Al}) - \frac{Q_{c,TEM}}{A_{TEM} th_{Al}} \tag{9}$$

$$\mathrm{Gr}_{panel-room} = \frac{g\beta (T_{surf} - T_{room}) L_c^3}{\nu_{air}^2} \tag{10}$$

$$\mathrm{Ra}_{panel-room} = \mathrm{Gr}_{panel-room} \times \mathrm{Pr}_{air} \tag{11}$$

$$\mathrm{Nu}_{panel-room} = 0.27\mathrm{Ra}^{1/4} \qquad (10^5 < Ra < 10^{11}) \tag{12}$$

$$h_{panel-room} = \frac{\kappa_{air} Nu_{panel-room}}{L_c} \tag{13}$$

The governing equation for the surface that was not directly facing the TEM (point 2, Figure 2) is presented in Eq. (14). The overall heat transfer coefficient between the panel surface and air in the duct ($U_{panel-duct}$) can be derived using Eq. (15). It included the thermal resistances of the aluminum panel, copper panel, thermal insulation, and heat convection coefficient between air and the air in the duct and the surface of insulation ($h_{duct-ins}$) calculated using Eqs. (16) to (19). The Nusselt number was determined according to the Reynolds number (Eq. (16)) and the Prandtl number using Eqs. (17) and (18), respectively (Churchill and Ozoe, 1973; Thomas, 1977). The effect of the velocity boundary layer was assumed to be negligible because of the low heat convection coefficient between the duct and the thermal insulation.

$$\rho_{Al} C_{p,Al} \frac{\partial T}{\partial t} = \kappa_{Al} \left(\frac{\partial^2 T}{\partial x^2} + \frac{\partial^2 T}{\partial y^2}\right) + \frac{h_{panel-room}}{th_{Al}} (T_{room} - T_{Al}) + \frac{U_{panel-duct}}{th_{Al}} \left(T_{a,duct} - T_{Al}\right) \tag{14}$$

$$U_{panel-duct} = \left(\frac{th_{Al}}{\kappa_{Al}} + \frac{th_{Cu}}{\kappa_{Cu}} + \frac{th_{ins}}{\kappa_{ins}} + \frac{1}{h_{duct-ins}}\right)^{-1} \tag{15}$$

$$\mathrm{Re}_{duct} = \frac{\rho_{air} v_{duct} L_c}{\mu_{air}} \tag{16}$$

$$\mathrm{Nu}_{duct-ins} = 0.664\mathrm{Re}_{duct}^{1/2} Pr_{air}^{1/3} \qquad (\mathrm{Pr} > 0.6, Re < 5) \tag{17}$$

$$\mathrm{Nu}_{duct-ins} = 0.037\mathrm{Re}_{duct}^{0.8} Pr_{air}^{1/3} \quad (0.6 \le \mathrm{Pr} \le 60, 5 \times 10^5 \le Re \le 10^7) \tag{18}$$

$$h_{duct-ins} = \frac{\kappa_{air} Nu_{duct-ins}}{L_c} \tag{19}$$

The time derivation, x-direction derivation, and y-direction derivation were described in Eqs. (20) to (22), respectively, to numerically solve Eqs. (9) and (14). Consequently, two governing equations for the TEM-RCP were derived in Eqs. (24) and (25).

$$\frac{\partial T}{\partial t} = \frac{T_{i,j}^{t+1} - T_{i,j}^{t}}{\Delta t} \tag{20}$$

$$\frac{\partial^2 T}{\partial x^2} = \frac{T_{i-1,j}^{t} - 2T_{i,j}^{t} + T_{i+1,j}^{t}}{\Delta x^2} \tag{21}$$

$$\frac{\partial^2 T}{\partial y^2} = \frac{T_{i,j-1}^{t} - 2T_{i,j}^{t} + T_{i,j+1}^{t}}{\Delta \mathrm{y}^2} \tag{22}$$

$$\mathrm{M} = \frac{\rho_{Al} C_{p,Al} (\Delta x^2 \Delta y^2)}{\kappa_{Al} \Delta t} \tag{23}$$

$$T_{i,j}^{t+1} = \frac{T_{i-1,j}^{t} + T_{i+1,j}^{t} + T_{i,j-1}^{t} + T_{i,j+1}^{t} + (M-4)T_{i,j}^{t}}{M} + \frac{\Delta t}{\rho_{Al} C_{p,Al}} \left(\frac{h_{panel-room}}{th_{Al}} (T_{room} - T_{Panel}) - \frac{Q_{c,TEM}}{A_{TEM} th_{Al}} \right) \tag{24}$$

$$T_{i,j}^{t+1} = \frac{T_{i-1,j}^{t} + T_{i+1,j}^{t} + T_{i,j-1}^{t} + T_{i,j+1}^{t} + (M-4)T_{i,j}^{t}}{M} + \frac{\Delta t}{\rho_{Al} C_{p,Al}} \left(\frac{h_{panel-room}}{th_{Al}} (T_{room} - T_{Panel}) + \frac{U_{panel-duct}}{th_{Al-duct}} \left(T_{a,duct} - T_{panel} \right) \right) \tag{25}$$

4. RESULTS

4.1 Simulation results

The effects of the interval between the TEMs and the arrangement of the TEMs on the temperature distributions of the TEM-RCP were investigated through a simulation. First, the temperature distributions according to the interval between the TEMs were estimated. The design condition was determined based on the room and outdoor air condition of summer in Seoul, South Korea. We simulated the minimum area for estimating the temperature distribution of the TEM-RCP to reduce the calculation time. The simulated area was the square of the interval between the TEMs. The room air temperature was assumed to be 26°C. The temperature and the air flow rate of the outdoor air for heat rejection were 30°C and 500 m^3/h, respectively. The air flow rate was set as the maximum value of the fan we planned to use in the experiment. The surface temperature of the aluminum panel was set as 16°C considering the dew point temperature of the room. The thickness of the aluminum and copper panels was 3 and 2 mm, respectively. The cooling load was assumed to be 63.6 W, which was 60% of the maximum cooling capacity of the TEM. The simulation was conducted for 5 min with a second interval. The nodes for the x- and y- directions were 11 (i.e., a total of 121 nodes). The minimum interval satisfying the maximum temperature difference of 3°C across a given grid was investigated (American Society of Heating, Refrigerating and Air-Conditioning Engineers (ASHRAE), 2013). Figure 4 plots the temperature distributions of the TEM-RCP according to the intervals with ranges 0.28 to 0.38. In the design condition, 0.28 m was the minimum interval between the TEMs for the TEM-RCP.

Second, the temperature distributions of the TEM-RCP according to the TEM arrangement were evaluated. We selected triangular and rectangular grids and used a 0.28 m interval. As a result, the triangular and rectangular grids showed the maximum temperature differences of 2.9°C and 3.1°C, respectively. The rectangular grid used one more TEM in the same area for cooling. Meanwhile, the temperature distribution of the triangular grid was more uniform. Therefore, the triangular grid with the 0.28 m interval between the TEMs was used for the mock-up model of the TEM-RCP.

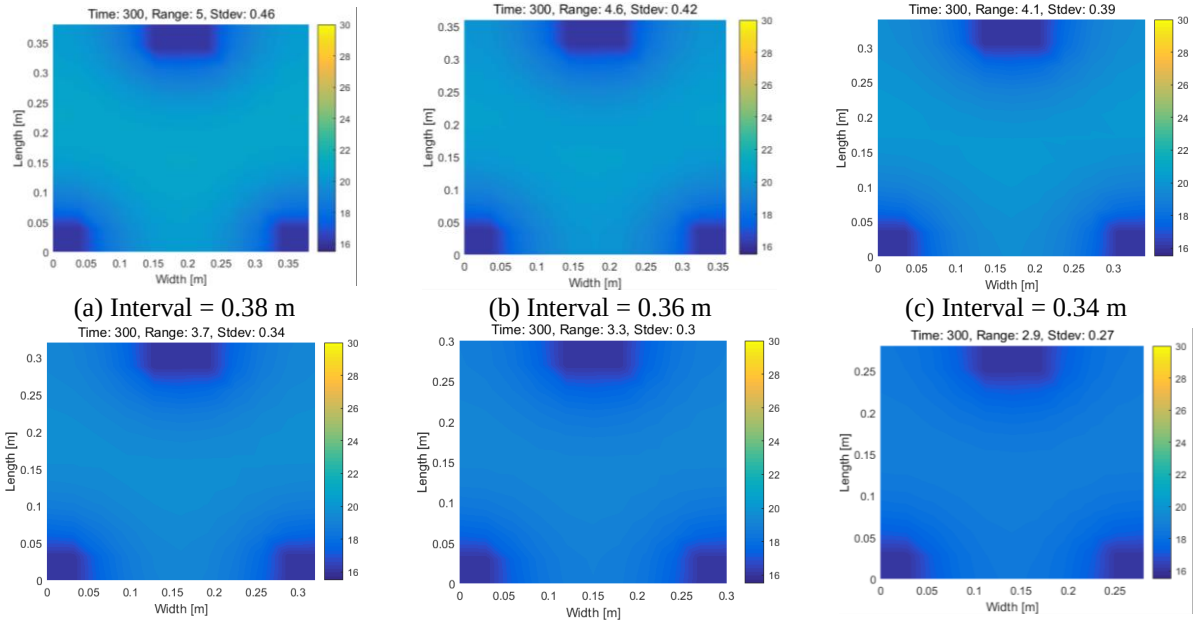

(a) Interval = 0.38 m (b) Interval = 0.36 m (c) Interval = 0.34 m

(d) Interval = 0.32 m (e) Interval = 0.30 m (f) Interval = 0.28 m

Figure 4: Temperature distribution of the thermoelectric module radiant cooling panel according to the interval between the thermoelectric modules

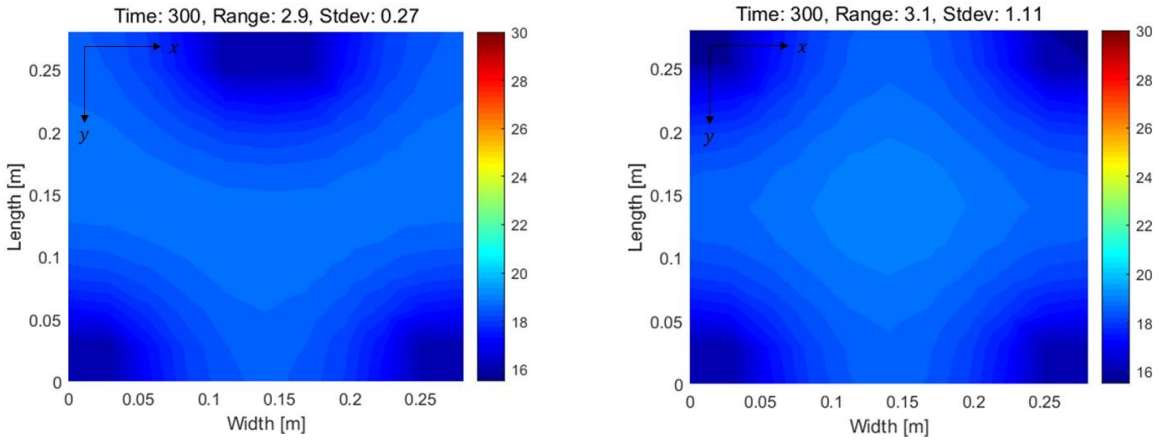

(a) Triangular grid (b) Rectangular grid

Figure 5: Comparison of the temperature distributions according to the arrangement

4.2 Validation results

The mock-up model of the TEM-RCP was designed for the validations (Figure 6). The designed TEM-RCP for the in situ experiments had the same cross-sectional plans with that in Figure 3. We used seven TEMs for the experiments. The distance between the TEMs was 0.28 m in the longitudinal direction and 0.24 m in the lateral direction. The interval and the arrangement of the TEMs were determined based on the simulation results in Section 4.

The plenum size was 0.6 m (width) × 1.2 m (length) × 0.3 m (height). The side wall of the plenum was integral with the aluminum panel. The plenum cover was transparent acrylic and can be separated for maintenance. The flexible duct with a diameter of 150 mm was connected using transition and flange. The direct current (DC) power for the TEM was supplied using the switched mode power supply to control the input current and voltage. The power was distributed to the TEMs using a DC power terminal block.

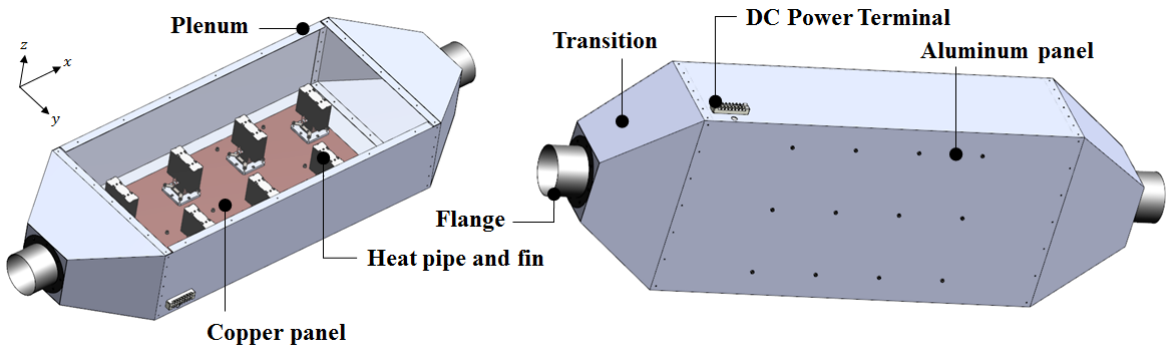

Figure 6: 3D model of the thermoelectric module radiant cooling panel for the in situ experiment

Figure 7 shows the constructed TEM-RCP. We attached the compressed polystyrene foam around the plenum for the thermal insulations. Teflon insulations were then attached between the air plenum and the copper panel to reduce the heat transfers. The conditioned air was entered into the plenum for heat rejection during the TEM-RCP operations using an environmental chamber.

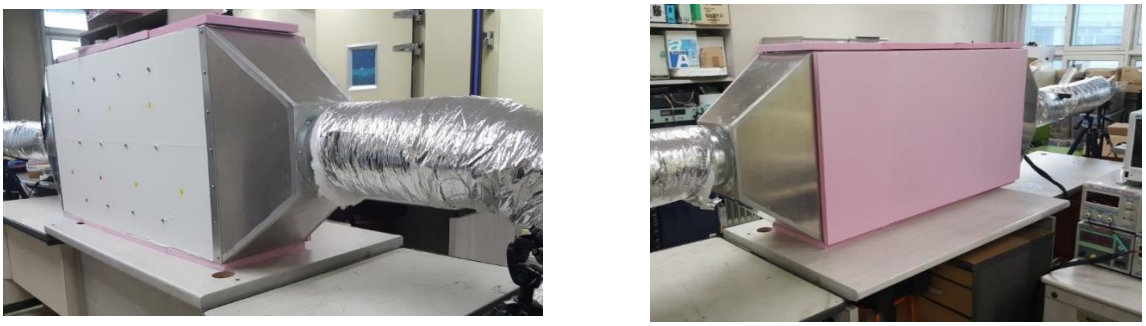

(a) Front view (b) Rear view

Figure 7: Mock-up model of the thermoelectric module radiant cooling panel

The temperature distributions of the TEM-RCP were measured using an infrared camera for thermal images (Testo 882) to validate the simulation model. The TEM-RCP was tested in the vertical installation for measuring convenience. The TEM was operated under 4 A and 24.5 V when the air for heat rejection was 30°C, and the air flow rate was 300 m^3/h. The room temperature for radiant cooling was 20°C, and no forced air was involved. Figure 8 depicts the comparison of the measurement and the simulation. The temperature distributions between the two TEMs (i.e., TEM 1 and TEM 2) showed a similar pattern. However, TEM 3 showed a higher temperature compared with the simulation results because the experiment was performed in the vertical installation; therefore, the air flow was not uniformly distributed in the y-directions, and the heat at TEM 3 was not sufficiently rejected.

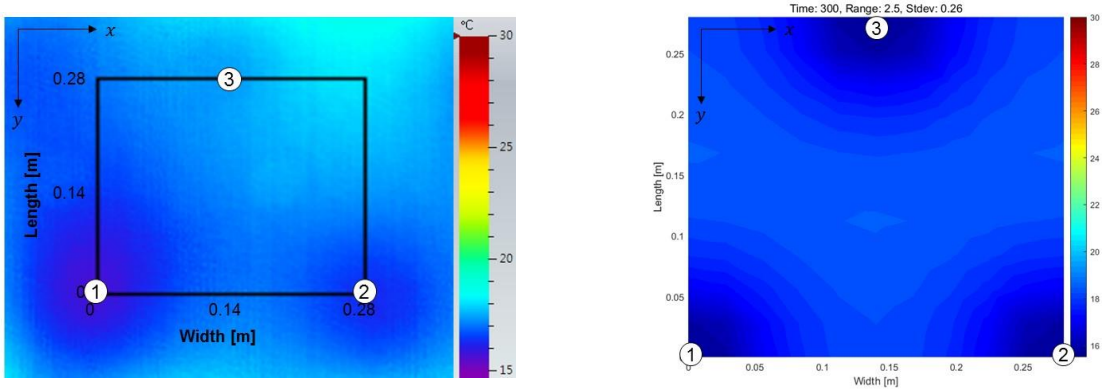

(a) Measurement results (b) Simulation results

Figure 8: Comparison of the temperature distribution of the thermoelectric module radiant cooling panel

The temperature values of the measured area were quantitatively summarized in Figure 9 using a histogram. The maximum and minimum temperature were 18.1 and 15.6°C, respectively. The maximum and minimum temperatures of the simulation results were similar. Therefore, we can conclude that the simulation showed reliable results compared to the in situ measured temperature distributions.

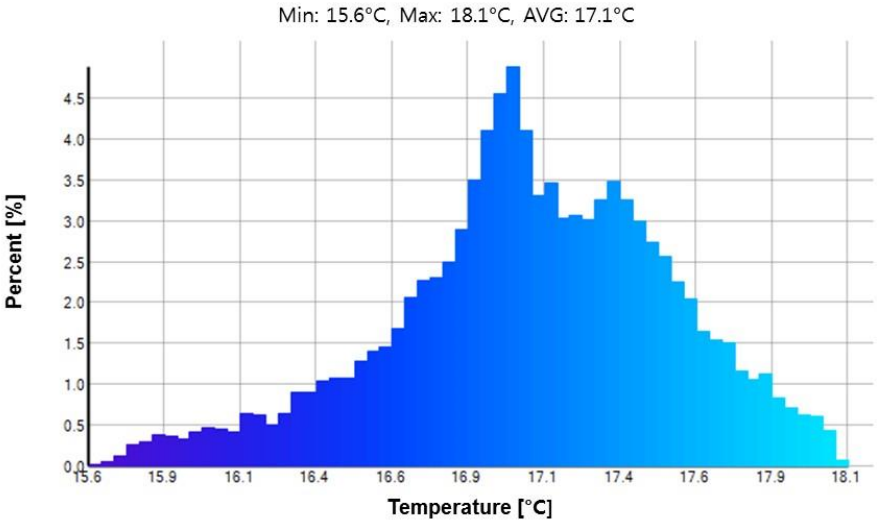

Figure 9: Histogram of the measured surface temperatures between the three thermoelectric modules

6. TEM-RCP DESIGN TOOL IN THE GUI

The GUI was applied to provide an easy-to-use simulation tool for the TEM-RCP (Figure 10). The GUI programming tool in MATLAB was used. There are three parts for input setting regarding the zone condition, characteristics of TEM, and panel. The geometric node was fixed, and the duration for the simulation can be adjusted. The results were plotted in 2D color contour maps for the temperature. The time, maximum temperature difference of the TEM-RCP, and standard deviation of the temperature values on the surface were plotted. The COP of the TEM for cooling, optimized interval between the TEMs, required power, including the fan, and required air flow rate of the outdoor air for heat rejection were also provided.

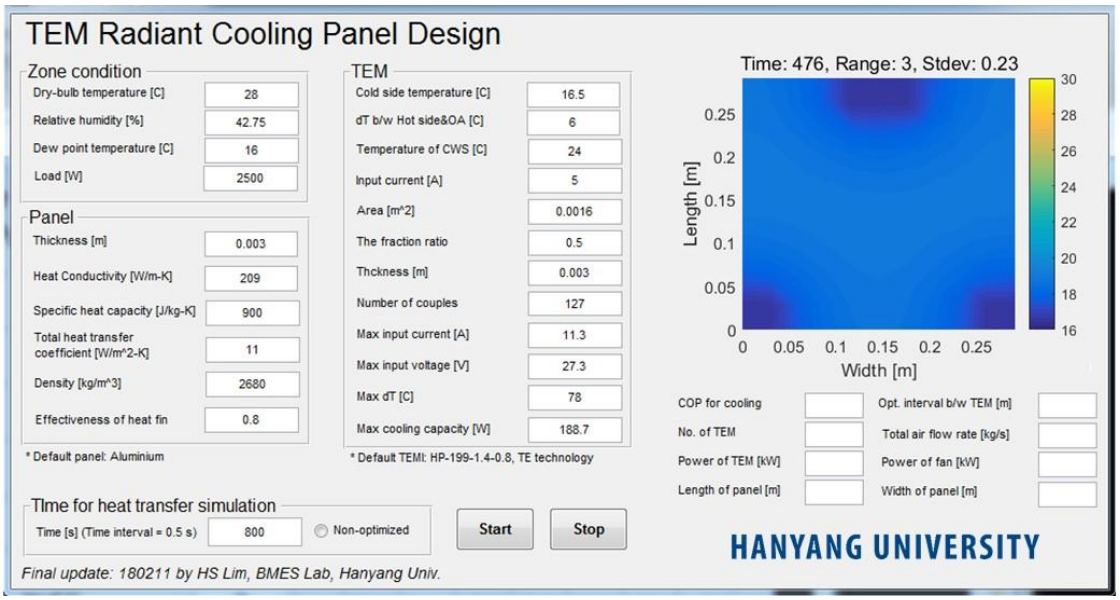

Figure 10: GUI simulation program for designing the TEM-RCP

6. CONCLUSIONS

This study developed and validated the numerical FDM simulation model for the TEM-RCP based on the experiment. For validation, a mock-up model of the TEM-RCP was constructed with a maximum cooling capacity of 742 W. The TEM-RCP was an air-cooled type system for heat rejection at the hot side of the TEM and the outdoor air was used. The interval and the arrangement between the TEMs were investigated for an even surface temperature distribution of the TEM-RCP using the simulation model. As a result, the 0.28 m interval was found to be appropriate for satisfying the guideline from the ASHRAE Handbook under the summer condition. The temperature distribution of the TEM-RCP was also investigated when the TEMs were in the rectangular and triangular grids. The results showed that the triangular grid can generate a more even temperature distribution with less number of TEMs compared with the rectangular grid. In a further study, various TEM arrangements will be investigated, and the experiments for verifying the numerical FDM simulation model for the TEM-RCP will be conducted in more detail to reveal the characteristics of the in situ TEM-RCP. The improvement of the GUI simulation design tool will also be continued such that it can be used for various TEM-RCP configurations.

NOMENCLATURE

α	Seebeck coefficient of the thermocouple	(V/K)
A_{TEM}	Area of TEM	(m^2)
β	Coefficient of cubical expansion	(1/°C)
C_p	Specific heat capacity	(kJ/kg·°C)
Δ	Difference	(–)
f_p	Packing fraction of the total TEM	(–)
g	Acceleration of gravity	(m/s^2)
Gr	Grashof number	(–)
h	Heat convection coefficient	($W/m^2 \cdot K$)
I	Current	(A)
κ	Thermal conductance of the thermocouple	(W/K)
K	Thermal conductance of TEM	(W/K)
l	Height of the thermoelement	(m)
L_c	Characteristic length	(m)
μ	Viscosity	(kg/ms)
n	Number of TEMs	(–)
N	Number of thermocouples	(–)
Nu	Nusselt number	(–)
P	Electrical power	(W)
Pr	Prandtl number	(–)
$\dot{Q}$	Thermal energy	(W)
ρ_{Al}	Density of aluminum	(kg/m^3)
ρ	Electrical resistance of the thermocouple	(Ω)
R	Electrical resistance of the TEM	(Ω)
Ra	Rayleigh number	(–)
Re	Reynold number	(–)
S	Seebeck coefficient of the TEM	(V/K)
T	Temperature	(°C)
th	Thickness	(m)
U	Overall heat transfer coefficient	($W/m^2 \cdot K$)
v	Velocity	(m/s)
V	Voltage	(V)

Subscript

air	Air
Al	Aluminum panel
c	Cold

Cu	Copper panel
duct	Duct
duct-ins	Between the duct and thermal insulation
h	Hot
i	Node in the x-direction
ins	Thermal insulation
j	Node in the y-direction
max	Maximum
panel-room	Between the panel and the room air
panel-TEM	Between the panel and the TEM
surface	Surface
t	Time
TEM	Thermoelectric module

REFERENCES

Jeong, J. W., Mumma, S. A., & Bahnfleth, W. P. (2003). Energy conservation benefits of a dedicated outdoor air system with parallel sensible cooling by ceiling radiant panels. *ASHRAE Trans., 109 Part 2*, 627–636.
Kim, M. H., Yoon, D. S., Kim, H. J., & Jeong, J. W. (2016). Retrofit of a liquid desiccant and evaporative cooling-assisted 100% outdoor air system for enhancing energy saving potential. *Appl. Therm. Eng., 96*, 441–453.
Liu, Z.B., Zhang, L., & Gong, G. C. (2014). Experimental evaluation of a solar thermoelectric cooled ceiling combined with displacement ventilation system. *Energy Convers. Manag., 87*, 559–565.
Lim, H., Shin, J., Li, S. Cho, H. J., & Jeong, J. W. (2017). Energy performance prediction of thermoelectric ceiling radiant panels with a dedicated outdoor air system. *Proceedings of the 38th AIVC — 6th TightVent & Venticool Conference, Nottingham, United Kingdom* (613–621).
Luo, Y., Zhang, L., Liu, Z., Wang, Y., Wu, J., & Wang, X. (2016). Dynamic heat transfer modeling and parametric study of thermoelectric radiant cooling and heating panel system. *Energy Convers. Manag., 124*, 504–516.
Shen, L., Tu, Z., Hu, Q., Tao, C., & Chen, H. (2017). The optimization design and parametric study of thermoelectric radiant cooling and heating panel. *Appl. Therm. Eng., 112*, 688–697.
Lee, H. S. (2016). *Thermoelectrics: Design and Materials*. Hoboken, NJ: John Wiley & Sons.
Chen, M., & Snyder, G. J. (2013). Analytical and numerical parameter extraction for compact modeling of thermoelectric coolers. *Int. J. Heat Mass Transf., 60*, 689–699.
Cengel, Y. A. *Heat and Mass Transfer: Fundamentals and Applications*. New York, NY: McGraw-Hill Education.
Ostrach, S. (1953). An analysis of laminar free-convection flow and heat transfer about a flat plate parallel to the direction of the generating body force. *National Advisory Committee for Aeronautics, Report 1111*.
Fujii, T., & Imura, H. (1972). Natural-convection heat transfer from a plate with arbitrary inclination. International *Journal of Heat and Mass Transfer, 15(4)*, 755–767.
Churchill, S. W., & Ozoe, H. (1973). Correlations for laminar forced convection in flow over an isothermal flat plate and in developing and fully developed flow in an isothermal tube. *Journal of Heat Transfer, 95(3)*, 416–419.
Thomas, W. C. (1977). Note on the heat transfer equation for forced convection flow over a flat plate with an unheated starting length. *Mechanical Engineering News, 9(1)*, 361–368.
American Society of Heating, Refrigerating, and Air Conditioning Engineers. (2013). Chapter 6: Panel heating and cooling., *Handbook: HVAC Systems and Equipment*, Atlanta, GA.

ACKNOWLEDGMENT

This work was supported by the Korea Agency for Infrastructure Technology Advancement (KAIA) grant (17CTAP-C116268-02), and the Korea Institute of Energy Technology Evaluation and Planning (KETEP) (No. 20164010200860).